Journal of Applied Polymer Science

Effects of Dodecyl Amine Functionalized Graphene Oxide on the Crystallization Behavior of Isotactic Polypropylene

Hao Wang,[1,2] Peng-Gang Ren,[1,2] Yan-Hui Chen,[3] Ding-Xiang Yan,[3] Zhong-Ming Li,[3] Ling Xu[2]

[1]Institute of Printing and Packaging Engineering, Xi'an University of Technology, Xi'an, Shaanxi 710048, People' Republic of China
[2]State Key Laboratory of Polymer Materials Engineering, Sichuan University, Chengdu, Sichuan 610065, People' Republic of China
[3]State Key Laboratory of Polymer Materials Engineering, College of Polymer Science and Engineering, Sichuan University, Chengdu, Sichuan, 610065, People' Republic of China
Correspondance to: P.-G. Ren (rengpg@126.com); L. Xu (xulingshannon@gmail.com)

ABSTRACT: Dodecyl amine functionalized graphene oxide (DA-GO)/isotactic polypropylene (iPP) nanocomposites were prepared via solution mixing method. Fourier transform infrared (FTIR), thermogravimetric analysis (TGA), and X-ray photoelectron spectroscopy (XPS) verified that the DA was successfully grafted onto the surface of graphene oxide. The crystallization behavior of iPP/DA-GO nanocomposites was investigated by differential scanning calorimetry (DSC) and polarized optical microscope (POM). The DSC results of both isothermal and non-isothermal crystallization process indicated that the addition of DA-GO can decrease the half-time crystallization ($t_{1/2}$) and elevate crystallization peak temperature (T_p) of iPP. The results of isothermal crystallization kinetics showed that the overall crystallization rates of iPP/DA-GO nanocomposites, especially with higher DA-GO content, were much faster than that of neat iPP. During the non-isothermal crystallization process, the nucleation ability (Φ) of nanocomposites containing 0.05, and 0.5 wt % DA-GO were 0.83 and 0.69, respectively. And the crystallization activation energy ΔE_a of iPP decreased from 348.7 (neat iPP) to 309.2 and 283.1 kJ/m^2 by addition of 0.05 and 0.5 wt % DA-GO, respectively. The decrease of Φ and $\ln t$ indicated DA-GO has strong heterogeneous nucleation effect and can promote the crystallization of iPP significantly. Additionally, POM micrographs showed the DA-GO in iPP matrix can form more nucleation sites for the spherulite growth. © 2013 Wiley Periodicals, Inc. J. Appl. Polym. Sci. **2014**, *131*, 40000.

KEYWORDS: dodecyl amine grafted graphene oxide; polyolefin; nanocomposites; crystallization; nucleating effect; kinetics

Received 11 June 2013; accepted 23 September 2013
DOI: 10.1002/app.40000

INTRODUCTION

The incorporation of organic and inorganic nanofillers into polymer matrices is of scientific and industrial interest because of their enhanced properties, reduced cost, as well as wide range of applications.[1–3] Among most reinforcement nanofillers, graphene has attracted a great deal of attention due to its unique structure and excellent properties.[3,4] It has been demonstrated that the presence of graphene in polymer matrices can greatly improve the properties of nanocomposites, such as mechanical, thermal stability, electrical conductivity, and gas barrier properties, etc.[5–7] The preparation of such nanocomposites requires that graphene sheets homogeneously distributed in the matrix. Unfortunately, graphene sheets are hydrophobic and easily agglomerate in many organic solvents which make them hardly be dispersed in polymer matrix.[8,9] So far, the production of nanocomposites from graphene oxide (GO) is still considered as an effective way to produce graphene based nanocomposite. GO, a precursor of graphene, bearing plenty of oxygen containing functional groups,[10,11] can be well dispersed in some polar solvents, such as water, *N*,*N*-dimethylformamide, and tetrahydrofuran, etc,[12] and polar polymer matrix. Thence, it is easy to obtain uniform dispersed GO/ polar polymer nanocomposites.[13–15] However, GO can hardly be dispersed in non-polar polymer, especially in polyolefin matrix with the hydrophilic groups. Therefore, the wide application of graphene as reinforcing filler in polyolefin nanocomposites is limited.

On the basis of modification, GO by grafting hydrophobic molecules on its surface, can be uniformly dispersed in polyolefin matrix via the solution mixing method. Several studies have demonstrated that alkyl functionalized GO can be well dispersed in polyethylene matrix and the properties of its nanocomposites are significantly improved.[16–19] Since polypropylene (PP) is one of the most widely used polymers, large amounts of studies have demonstrated that the properties of PP have been improved with incorporating nanofiller into its matrix,[20–23] few work focus on the study of functionalized GO filled PP

nanocomposites. It is noteworthy to mention that the properties of PP are significantly dependent on the crystallinity and crystalline structure.[24–27] Studies have shown that GO has strong nucleation ability and can accelerate crystallization process of PP.[28,29] However, no detailed study has paid attention to the crystallization behavior of alkyl functionalized GO/PP nanocomposites.

In this study, GO was modified by the amidation reaction with dodecyl amine (DA) and then the uniformly dispersed isotactic polypropylene/DA-GO (iPP/DA-GO) nanocomposites were obtained by the solution mixing method. The main objective of this paper is to investigate the crystallization behavior of iPP with the presence of DA-GO. Several crystallization kinetics (including Hoffman–Lauritzen theory, Dobreva and Gutzow method, as well as Kissinger equation) were employed to describe the crystallization ability of iPP/DA-GO nanocomposites. Moreover, spherulite growth behavior was also investigated using polarized optical microscopy (POM)

EXPERIMENTAL

Materials

iPP (model S1003, melt flow rate 3 g/10 min (230°C, 21.6 N), density 0.905 g/cm^3, $M_w = 3.4 \times 10^5$ g/mol and $M_w/M_n = 3.8$) was provided by Dushanzi Petroleum Chemical Co., China. Expandable graphite (KP 9950 250, ash content 1.0%, moisture content 1.0%, particle size 280 μm, expanded volume 250 mL/g) was supplied by Qingdao Haida Graphite Co., China. Dodecyl amine (DA), xylene, and ethanol were purchased from Chengdu Kelong Chemical Reagent Factory, China. All reagents were used as received.

Preparation of Dodecyl Amine Functionalized Graphene (DA-GO)

GO was synthesized from the expanded graphite via modified Hummers method, the detailed process was introduced in our previous reports.[30,31] For surface modification, 0.4 g GO was dispersed in 200 mL distilled water (2 mg/mL) by ultrasonication for 1 h. About 1.2 g DA was dissolved in ethanol and the mixture was added to the GO dispersion followed by stirring for 24 h at room temperature. After the reaction, the resultant was washed repeatedly with a water–ethanol (1:1) mixture to remove the residual DA. The black solid powder was dried under vacuum at 60°C for 72 h to obtain dry powder of DA-GO.

Preparation of iPP/DA-GO Nanocomposites

For preparation of iPP/DA-GO nanocomposites, a calculated amount of DA-GO was dispersed in 200 mL xylene by ultrasonication for 50 min. Subsequently, the mixture of DA-GO/xylene was heated to 145°C in oil bath. About 20 g iPP was dissolved in DA-GO/xylene under constant stirring. After the iPP particles were completely dissolved, the mixture was added drop-wise into a large volume of stirred ethanol. The obtained coagulation of iPP/DA-GO nanocomposites were washed several times with ethanol and dried in vacuum at 60°C for 5 days to remove residual solvent, the final nanocomposite materials were obtained. iPP/DA-GO nanocomposites containing 0, 0.05, and 0.5 wt % of DA-GO were designated as neat iPP, iPP/DA-GO-5, and iPP/DA-GO-50, respectively.

Characterization

Fourier Transform Infrared (FTIR). FTIR spectra of GO and DA-GO were carried out using a Nicolet FTIR (400 MHz) spectrometer at room temperature over a frequency range of 4000–400 cm^{-1}. The samples were well milled with KBr and pressed into thin pellets.

Thermogravimetric Analysis (TGA). TGA of GO and DA-GO (about 8 mg) were carried out on a Q50 TGA (TA instruments) with a heating rate of 10°C/min from room temperature to 600°C under nitrogen atmosphere.

X-ray Photoelectron Spectroscopy (XPS). XPS analysis was performed with an XSAM800 (Kratos company, Britain) using Al $K\alpha$ radiation ($h\nu$ = 1486.6 eV); XPSpeak41 software was used to perform curve fitting and calculate the atomic ratios.

Differential Scanning Calorimetry (DSC). The study of isothermal and non-isothermal behaviors of neat iPP and iPP/DA-GO nanocomposites were carried out on DSC Q2000 (TA Instruments) under a nitrogen flow with samples of about 6 mg, which was calibrated by indium as the standard. As for the isothermal crystallization kinetics, the samples were melted at 200°C for 5 min in order to eliminate any thermal history of the material, then the melt was rapidly cooled at the rate of 50°C/min down to the designated crystallization temperatures (T_c:130, 131, and 132°C respectively) and maintained at the T_c until the completion of polymer crystallization. For non-isothermal crystallization, samples were first heated from room temperature to 200°C at the rate of 20°C/min and maintained for 5 min. Then, each sample was cooled to 40°C at cooling rates of 2, 5, 10, and 20°C/min, respectively.

Polarizing Optical Microscopy (POM). The spherulite morphology was observed by an Olympus BX51 polarizing optical microscopy (POM) (Olympus Co., Tokyo, Japan) with a hot stage Linkam CSS-450. The film samples (about 8 μm) were first heated from room temperature to 200°C for 5 min to remove thermal histories, and then cooled to 132°C at a rate of 30°C/min and maintained at least 20 min.

RESULTS AND DISCUSSION

Characterization of GO and DA-GO

Figure 1 depicts the FT-IR spectrum of GO and DA-GO. In Figure 1, clear enhancement of intensity at 2921/2852 cm^{-1} (C–H stretching vibrations of CH_2 and CH groups), reduction of intensity at 1097/1064 cm^{-1} (C–O–C stretching vibrations) and disappearance of peak at 1728 cm^{-1} are observed in the DA-GO, indicating the successful introduction of long alkyl chains onto GO nanosheets. Additionally, the appearance of new peaks at 1462 cm^{-1} (C–N stretch of amide) and 719 cm^{-1} (C–H deformation) in DA-GO spectrum imply that the epoxide group and the amine group can react at room temperature. Therefore, it is evident that GO was successfully modified by DA.

TGA curves of GO and DA-GO are shown in Figure 2. Compared with GO, the mass losses of adsorbed water at about 100°C in DA-GO is about 2.5 wt %, lower than that of GO (about 10 wt %), which indicates that the GO has been changed from hydrophilic to hydrophobic after treated with DA chains. More weight loss at 350°C and lower char yield of DA-GO (about 40 wt %) compared to that of GO imply the existence of alkyl chains on the graphite oxide plane. As a result, both

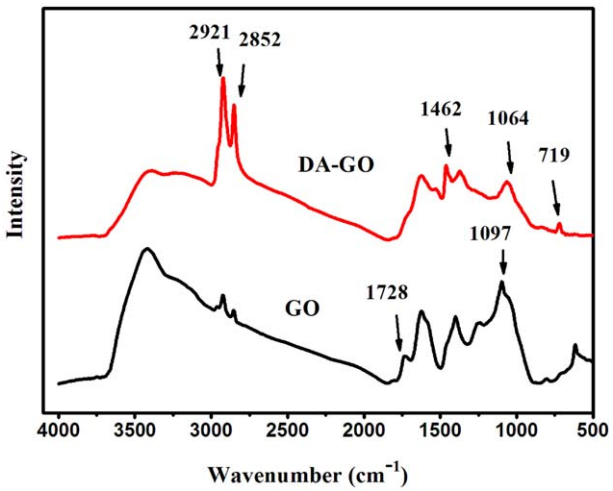

Figure 1. FT-IR spectrum of GO and DA-GO. [Color figure can be viewed in the online issue, which is available at wileyonlinelibrary.com.]

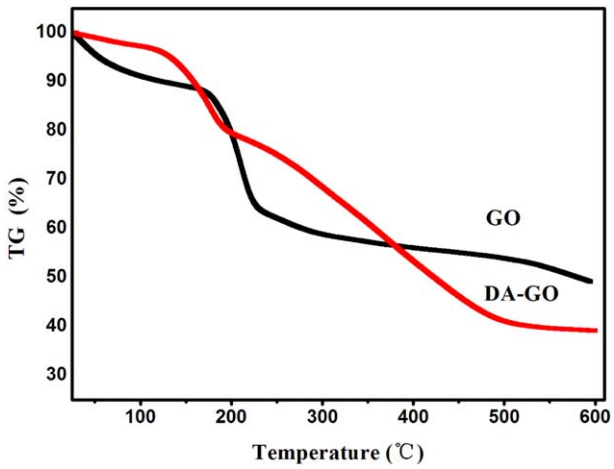

Figure 2. TG of GO and DA-GO. [Color figure can be viewed in the online issue, which is available at wileyonlinelibrary.com.]

FT-IR and TGA results demonstrate the DA molecule has been successful grafted on the GO sheets.

To further analysis the structure of DA-GO, the XPS analysis is employed. The C1*s* XPS spectrum of GO and DA-GO is depicted in Figure 3. It is clear that five different types of carbon with different chemical environments are observed in GO. The binding energies at 284.4, 285.7, 286.7, 288.0, and 289.1 eV are assigned to C–C/C=C, C–OH, C–O–C/epoxide group, C=O, and O–C=O, respectively. However, in the XPS spectrum of DA-GO [as shown in Figure 3(b)], obvious decrease of peak intensity at 286.8 eV indicates that the grafting reaction was mainly occurred on the epoxide groups of GO. Meanwhile, significant increase in peak intensity at 285.6 eV in DA-GO can be attributed to the formation of the C–N bond. All of those changes indicate the reaction of GO with DA.

Isothermal Crystallization Kinetics of iPP/DA-GO Nanocomposites

The typical isothermal crystallization curves of iPP and its DA-GO nanocomposites at different crystallization temperatures (T_c) are shown in Figure 4. It can be seen that the crystallization of iPP is strongly affected by T_c. As T_c increased, the crystallization exothermic peaks become flatter and shift to a higher value, meanwhile the time to complete crystallization is also increased. This indicates a longer crystallization time at a higher crystallization temperature.[32] At the same T_c, the crystallization exothermic peaks of iPP/DA-GO-50 nanocomposite appears first, followed by iPP/DA-GO-5 and neat iPP, which indicates the DA-GO exhibits a strong heterogeneous nucleating ability in the iPP matrix, and the nucleation effect is further enhanced with the increase of DA-GO content.

The relative degree of crystallinity (X_t), obtained from the area of the exothermic peak, is used to study the crystallization kinetics of iPP and its DA-GO nanocomposites. The plots of X_t as function of t time at various crystallization temperatures are shown in Figure 5. It can be seen that characteristic sigmoid isotherms of all the samples shift toward the right with increasing T_c, and shift toward the left with the increase of DA-GO content. This result suggests that the crystallization become faster with the decrease of T_c and the increase of DA-GO content. The value of half-time crystallization ($t_{1/2}$) corresponding to complete 50% of crystallization can be determined from Figure 5 and listed in Table I. It is clear that $t_{1/2}$ values of neat iPP nanocomposite is higher than that of iPP/DA-GO nanocomposites. $t_{1/2}$ of iPP at 132°C is 15.95 min, while the value of iPP/DA-GO-5 and iPP/DA-GO-50 are 11.66 and 4.91 min,

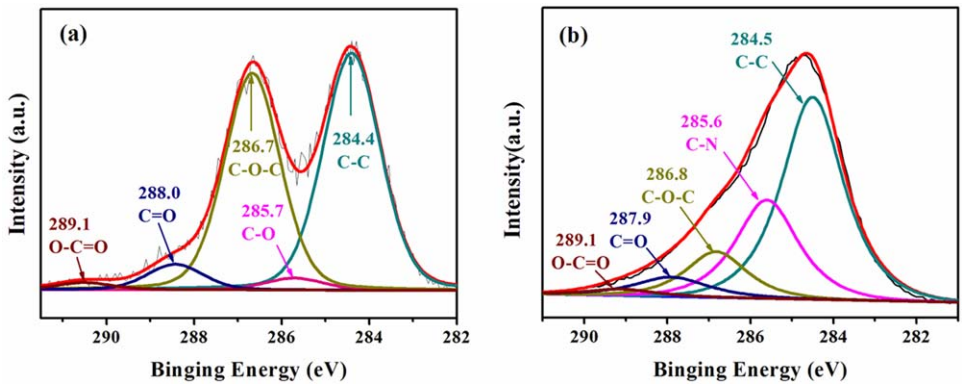

Figure 3. The C1*s* XPS spectra of (a) GO and (b) DA-GO. [Color figure can be viewed in the online issue, which is available at wileyonlinelibrary.com.]

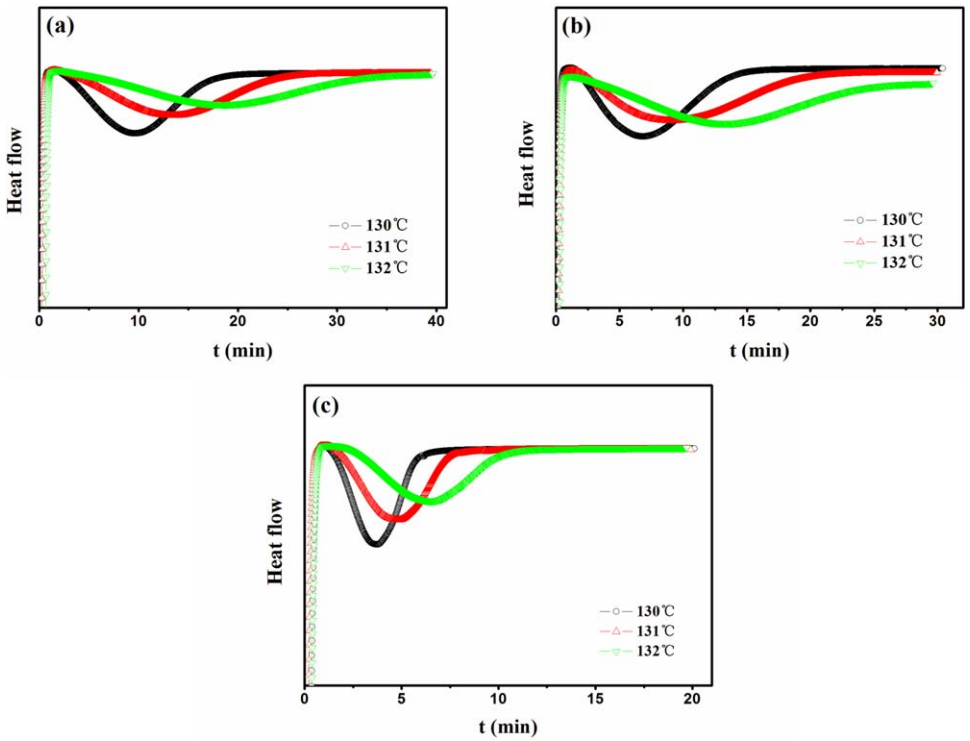

Figure 4. DSC curves of samples isothermally crystallized at the designated temperatures: (a) iPP; (b) iPP/DA-GO-5, and (c) iPP/DA-GO-50. [Color figure can be viewed in the online issue, which is available at wileyonlinelibrary.com.]

respectively, further verifying that DA-GO exhibits a strong heterogeneous nucleation ability and can accelerate the overall crystallization process of iPP.

To detailed analyze the isothermal crystallization kinetics of iPP/DA-GO nanocomposites, Avrami equation[33,34] is employed here, whose general form is given as follows:

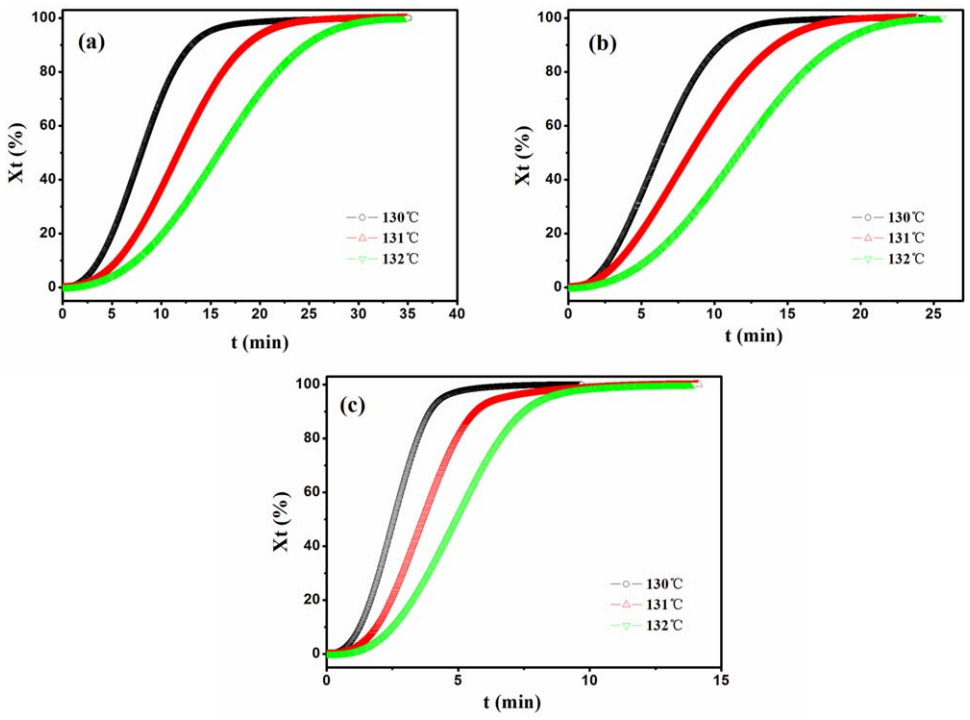

Figure 5. DSC curves of samples isothermally crystallized at the designated temperatures: (a) iPP; (b) iPP/DA-GO-5, and (c) iPP/DA-GO-50. [Color figure can be viewed in the online issue, which is available at wileyonlinelibrary.com.]

Table I. Isothermal Crystallization Kinetic Parameters for iPP and its Nanocomposites

Samples	T_c (°C)	$t_{1/2}$ (min)	n	K (min^{-1})	T_m (°C)	T_m^o (°C)	K_g (K^2)
	130	7.96	2.44	0.43×10^{-2}	166.2		
iPP	131	11.62	2.50	0.15×10^{-2}	166.5	185.6	5.3×10^5
	132	15.95	2.54	0.06×10^{-2}	166.9		
	130	6.20	2.33	0.98×10^{-2}	166.0		
iPP/DA-GO-5	131	8.22	2.35	0.75×10^{-2}	166.3	189.8	5.7×10^5
	132	11.66	2.48	0.15×10^{-2}	166.8		
	130	2.52	2.69	5.61×10^{-2}	165.9		
iPP/DA-GO-50	131	3.64	2.78	1.92×10^{-2}	166.5	209.7	11.6×10^5
	132	4.91	2.83	0.74×10^{-2}	167.0		

$$1-X_t=\exp\left(-Kt^n\right) \quad (1)$$

where K is crystallization rate constant involving both nucleation and growth rate parameters and n is the Avrami exponent constant depending on the type of nucleation and growth mechanism. Figure 6 shows the plots of $\ln(-\ln(1-X_t))$ versus $\ln t$. By fitting the linear portion, the parameters n and K can be easily obtained and the results are shown in Table I. It can be observed from Table I that the value of n is in the range of 2.33–2.83, indicating the growth mode of iPP and its nanocomposites are two-dimensional growth.[29] For each sample, the crystallization rate constant K decreases with the increase of crystallization temperature. Additionally, at each given T_c, the value of K increases with DA-GO content increasing. At 130°C, the K of neat iPP is 0.43×10^{-2} min^{-1}, while the K of iPP/DA-GO-5 and iPP/DA-GO-50 are 0.98×10^{-2} and 5.61×10^{-2} min^{-1}, respectively. This illustrates the acceleration of the crystallization saturates with the increasing of DA-GO content.

The equilibrium melting temperature (T_m^o) of a polymer is the thermodynamic quantity which defines the melting temperature of an equilibrium crystal, i.e., of infinite size, of that polymer.[35] Therefore, to carry on the quantitative analysis of crystallization behavior, especially to investigate the temperature dependence of crystallization rate, it is necessary to determine the equilibrium melting point as accurately as possible.[36] According to the Hoffman–Weeks theory,[37] the equilibrium melting point may be deduced by an extrapolation of a linear fit of the T_m versus T_c plot to the line $T_m = T_c$, where the intercept value is taken as T_m^o. The T_m^o values of neat iPP and its nanocomposites are shown in Table I. The values of T_m^o are 185.6, 189.8, and 209.7°C for neat iPP, iPP/DA-GO-5, and iPP/DA-GO-50,

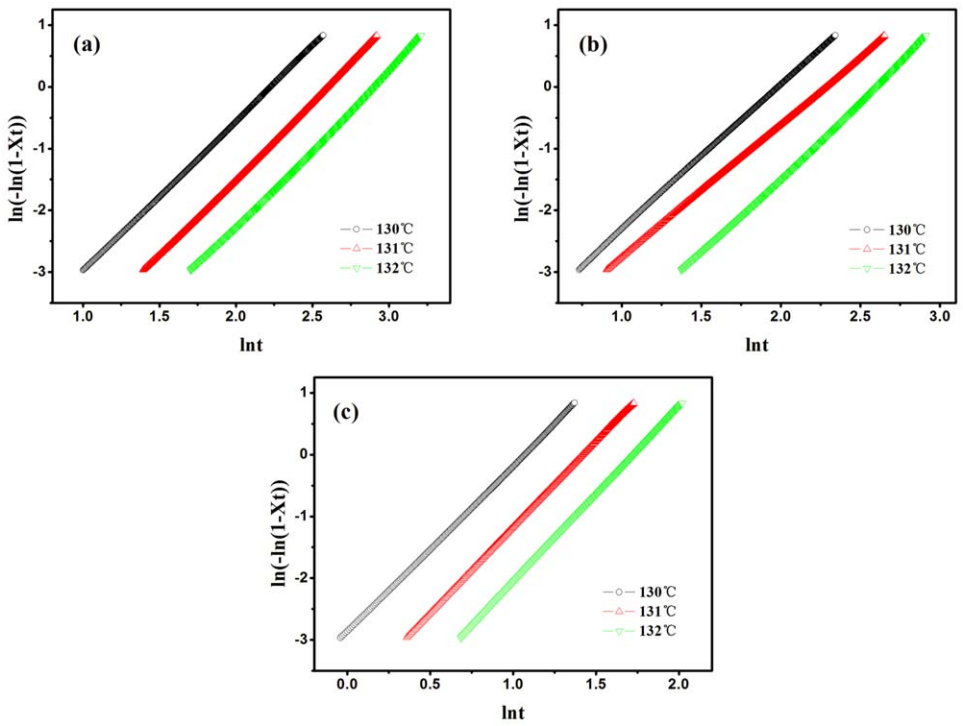

Figure 6. Plots of $\ln(-\ln(1-X_t))$ versus $\ln t$ during thermal crystallization process: (a) iPP; (b) iPP/DA-GO-5, and (c) iPP/DA-GO-50. [Color figure can be viewed in the online issue, which is available at wileyonlinelibrary.com.]

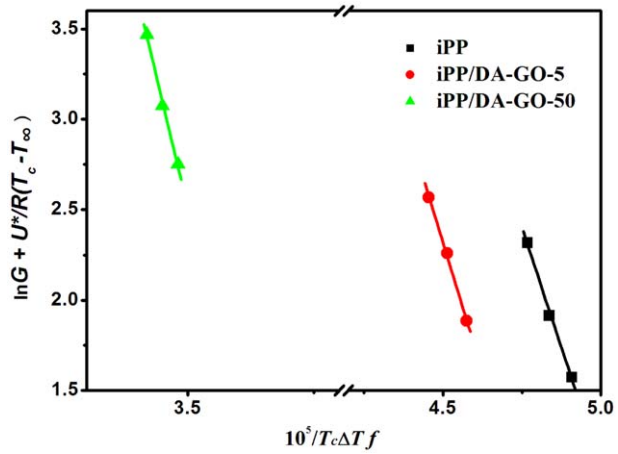

Figure 7. Hoffman–Lauritzen growth rate for iPP; DA-GO/iPP-5, and DA-GO/iPP-50. [Color figure can be viewed in the online issue, which is available at wileyonlinelibrary.com.]

respectively. Obvious increase of T_m^o with an increase in content of DA-GO in the nanocomposites indicates that high DA-GO content may lead to more perfect structure of crystals.[38,39]

To further describe the overall growth rate of crystallization, G, defined as $G = 1/(t_{1/2})$ can be expressed as follows according to the Hoffman and Lauritzen theory[40]:

$$G = Go \exp\left[-\frac{U^*}{R(Tc - T_\infty)}\right] \exp\left[-\frac{K_g}{T_c \Delta T f}\right] \quad (2)$$

where G_0 is a pre-exponential term; U^* is the diffusional activation energy for the transport of crystallizable segments at the liquid–solid interface, and the recommended values $U^* = 6280$ J/mol;[38] K_g is the secondary nucleation constant in a given regime; R is the universal gas constant; $T_\infty = T_g - 30$ is the hypothetical temperature, below which viscous flow ceases; T_g is the glass transition temperature of iPP and taken as 261.2 K;[41] ΔT is equal to $T_m^o - T_c$, T_m^o is equilibrium melting temperature and T_c is isothermal crystallization temperature, meanwhile, $f = 2T_c/(T_m^o + T_c)$.

The Hoffman–Lauritzen plot of $\ln G + U^*/R(T_c - T_\infty)$ against $1/(T_c \Delta T f)$ shows straight line for the neat iPP and its nanocomposites (as shown in Figure 7) and nucleation constant K_g is obtained from the slope (shown in Table I). The K_g of iPP/DA-GO-5 and iPP/DA-GO-50 are 5.7×10^5 and 11.6×10^5 K^2, respectively, obviously higher than that of iPP (5.3×10^5 K^2. This result may be explained by the strong heterogeneous nucleating effects of DA-GO.

Non-isothermal Crystallization Kinetics of iPP/DA-GO Nanocomposites

Since the common processing technology in industrial applications, such as extrusion and injection molding, is essentially a non-isothermal crystallization process, investigating non-isothermal crystallization of neat iPP and its nanocomposites are instructive.[28] The crystallization peak temperature (T_p) and the enthalpy of crystallization (ΔH_c) are presented in Table II. Apparently, the T_p value of iPP significantly increases with the addition of DA-GO (at cooling rate of 2°C/min, the T_p value of iPP is 121.8°C, while iPP/DA-GO-50 is 126.6°C). This phenomenon can be explained by strong heterogeneous nucleation effect of DA-GO on iPP crystallization, which can promote the crystallization of iPP at a higher temperature. Similar result is obtained from the value of ΔH_c. It can clearly be seen that the ΔH_c decreases as the cooling rate increases, while becomes higher when the DA-GO loading in the composites increases, ascribing to more perfect of crystallization induced by DA-GO nanosheets.

The relative degree of crystallinity (X_t) as a function of time t for iPP and its nanocomposites can be calculated as follows[38]:

$$X_t = \int_0^t \frac{dHc}{dt} dt \Big/ \int_t^{t\infty} \frac{dHc}{dt} dt \quad (3)$$

where dH_c is the enthalpy of crystallization released during an infinitesimal time interval dt. Plots of X_t as function of time t at different cooling rates are shown in Figure 8. It can be seen that the sigmoidal curves shift toward the left with the content of DA-GO at a given cooling rate owing to the presence of DA-GO can accelerate the crystallization of iPP. The time of 50% relative crystallinity ($t_{1/2}$) is an indicative of the crystallization rate of the polymer[29] and it can be obtained from the curves in Figure 8. Table II shows that $t_{1/2}$ of nanocomposites at the each given cooling rate is shorter than that of neat iPP, especially with higher DA-GO content. At a cooling rate of 2°C/min, the $t_{1/2}$ decreases from 4.63 to 2.44 min with 0.5 wt % DA-GO content. The significant decrease of $t_{1/2}$ is attributed to the nucleation sites provided by DA-GO. That is, higher DA-GO loading can provide plentiful nucleation sites so that the crystallization of iPP becomes faster with DA-GO content increases.

Since the crystallization process is divided into the nucleation and growth, the previous work has demonstrated that DA-GO can evidently accelerate the overall crystallization of iPP. To further understand the efficiency of DA-GO as a nucleator, the nucleation ability (Φ) was evaluated based on a method

Table II. Nonisothermal Crystallization Kinetic Parameters for iPP and its Nanocomposites

Samples	ϕ (°C/min)	T_p(°C)	ΔH_c (J/g)	$t_{1/2}$ (min)	Φ	ΔE_a (KJ/m^2
	2	121.8	105.2	4.63		
iPP	5	118.2	102.2	2.04		348.7
	10	115.6	99.29	1.15		
	20	113.3	96.32	0.57		
	2	123.6	107.7	3.83		
iPP/ DA-GO-5	5	119.9	105.1	1.69	0.83	309.2
	10	116.9	102.3	0.99		
	20	113.9	99.39	0.53		
	2	126.6	110.1	2.44		
iPP/ DA-GO-50	5	123.2	107.6	1.08	0.69	283.1
	10	120.4	104.7	0.66		
	20	117.6	102.6	0.35		

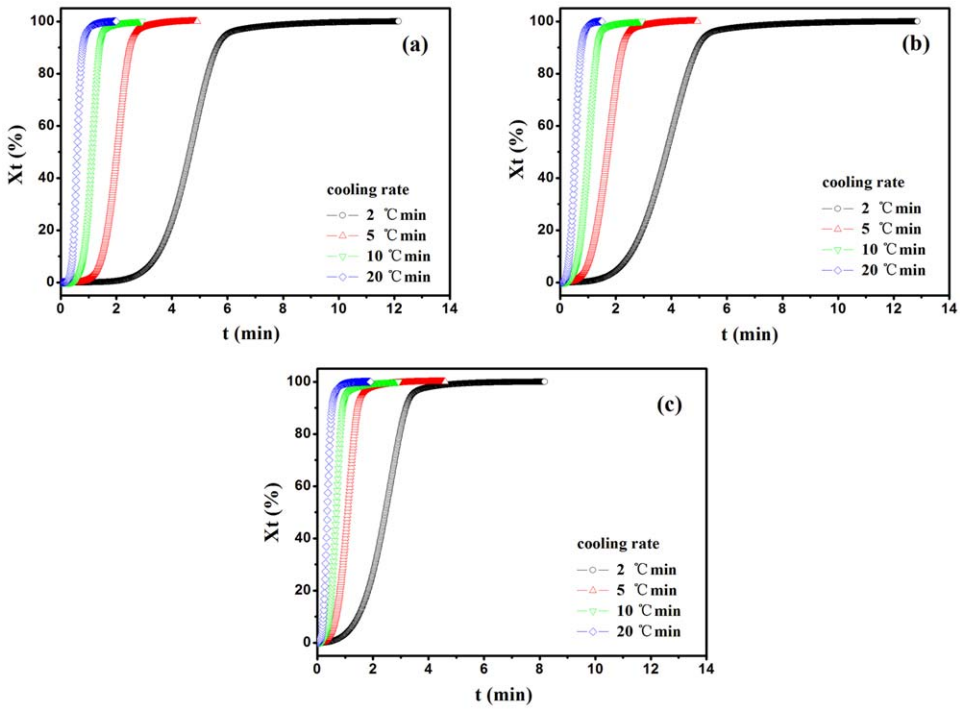

Figure 8. Plots of X_t versus t for (a) iPP; (b) iPP/DA-GO-5, and (c) iPP/DA-GO-50. [Color figure can be viewed in the online issue, which is available at wileyonlinelibrary.com.]

proposed by Dobreva and Gutzow.[42] The nucleating activity is calculated by the ratio as follows:

$$\Phi = \frac{B^*}{B} \tag{4}$$

where B is a parameter for homogeneous nucleation, while B^* is for heterogeneous nucleation. In the case of homogeneous nucleation, B can be determined from the slope of the following equation:

$$\ln \phi = \text{Constant} - \frac{B}{2.303\Delta T_p^2} \tag{5}$$

where ΔT_p denotes the degree of supercooling ($\Delta T_p = T_m - T_p$). For the heterogeneous case, B is replaced by B^*. The value of Φ varies from 0 to 1, and the more active the nucleator is, the lower the value of Φ should be. Plots of ln φ versus $10^4/\Delta T_p^2$ for neat iPP and its nanocomposites are shown in Figure 9. The slope of iPP, iPP/DA-GO-5, and iPP/DA-GO-50 are 10522, 8821, and 7308, respectively. Therefore, the corresponding Φ values of the nanocomposites containing 0.05 and 0.5 wt % DA-GO are 0.83 and 0.69, respectively. This result shows that DA-GO is an effective nucleating agent for iPP in the nanocomposites, and the higher DA-GO content the stronger of nucleation ability will be.

Considering the impact of different cooling rates on the nonisothermal crystallization behavior, the activation energy of crystallization was derived from the Kissinger equation as follows[43]:

$$\frac{d[\ln(\phi/T_p^2)]}{d((1/T_p)} = -\frac{\Delta E_a}{R} \tag{6}$$

where T_p is the temperature of crystallization exothermal peak, R the ideal gas constant, and ΔE_a the crystallization activation energy. Plots of $\ln(\phi/T_p^2)$ versus $1/T_p$ for neat iPP and its nanocomposites are shown in Figure 10, and ΔEa determined from the slope of these plots are presented in Table II. As observed, the calculated ΔEa values for iPP, iPP/DA-GO-5, and iPP/DA-GO-50 are 348.7, 309.2, and 283.1 kJ/m^2, respectively. Significant decrease of ΔEa values for DA-GO nanocomposites demonstrates the incorporation of DA-GO into iPP makes the transportation of iPP chain segments to the growing crystal surface easily. Additionally, the lowest ΔEa value of iPP/DA-GO-50 suggests that higher DA-GO content can provide sufficient

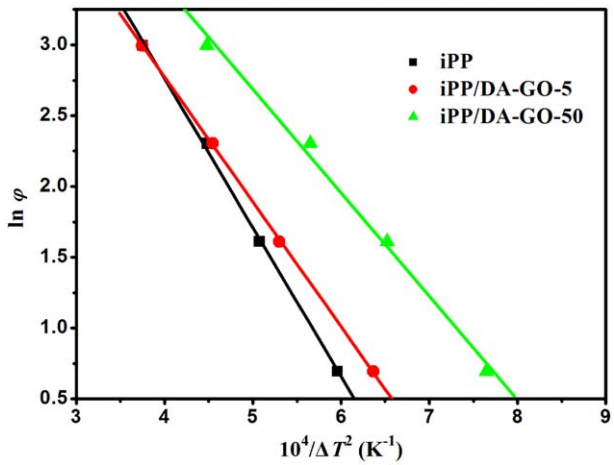

Figure 9. Plots of lnφ versus $10^4/\Delta T^2$ to determine the nucleation activity for non-isothermal crystallization of iPP, iPP/DA-GO-5, and iPP/DA-GO-50. [Color figure can be viewed in the online issue, which is available at wileyonlinelibrary.com.]

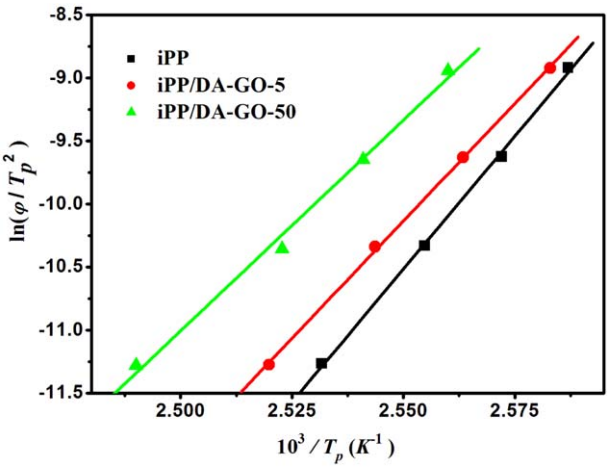

Figure 10. Plot of $\ln(\phi/T_p^2)$ versus $10^3/T_p$ for iPP, iPP/DA-GO-5, and iPP/DA-GO-50. [Color figure can be viewed in the online issue, which is available at wileyonlinelibrary.com.]

nucleating agents for iPP and thus reduce the barrier to nucleation caused by the surface interfacial free energy.

Spherulitic Growth

The effect of DA-GO in the iPP matrix as the nucleation agent on the isothermal crystallization behavior of iPP/DA-GO nanocomposites at 132°C is further observed using a polarized optical microscopy equipped with a hot stage (as shown in Figure 11). As presented in Figure 11, it is clear that the crystallization behavior of neat iPP and its nanocomposites are quite different. At the beginning of isothermally crystallizing (0 min), neat iPP shows relatively clean and uniform melt, while a few micro-scale nuclei can be observed in both iPP/DA-GO-5 and iPP/DA-GO-50 nanocomposites. This phenomenon is mainly due to the fact that the DA chain on GO sheet restricts the freedom movement of iPP chain, which in turn accelerates the arrangement of iPP chain onto GO sheet. After 4 min, the nucleus density of iPP/DA-GO nanocomposites crystallites significantly increase compared to that of neat iPP. And the number of nuclei in iPP/DA-GO-50 is much more than that of iPP/DA-GO-5 nanocomposite. This further illustrates the fact that DA-GO can promote the nucleation of iPP, and higher DA-GO content can form more nucleation sites for the spherulite growth. It is clear that the screen of iPP/DA-GO-50 has been nearly full of nuclei at 4 min. After 15 min of isothermal crystallization, it can be seen that the formed spherulites in iPP become larger and the average diameter is about 85 μm, while the spherulites in iPP/DA-GO-5 and iPP/DA-GO-5 nanocomposites have filled up the whole screen, the average diameter spherulites are respectively about 50 and 15 μm. Since the number of nuclei formed during a limited crystallization time may represent the nucleation rate of the sample,[44] the nucleation rate of iPP/DA-GO nanocomposites show a significant promotion compared to neat iPP, and which is in well agreement with the decrease of $t_{1/2}$ above.

The schematic diagram of crystallization process of iPP/DA-GO nanocomposite is shown in Figure 12. Since the compatibility between DA chain and iPP chain is not very well, the presence of DA chain restricts the freedom movement of iPP molecular chain nearby. Therefore, the iPP molecular chain is much easier to arrange onto GO sheet and mutual entangles nearby DA chain, and resulting in high crystallization rate due to lower interfacial free energy between iPP molecular chain and GO

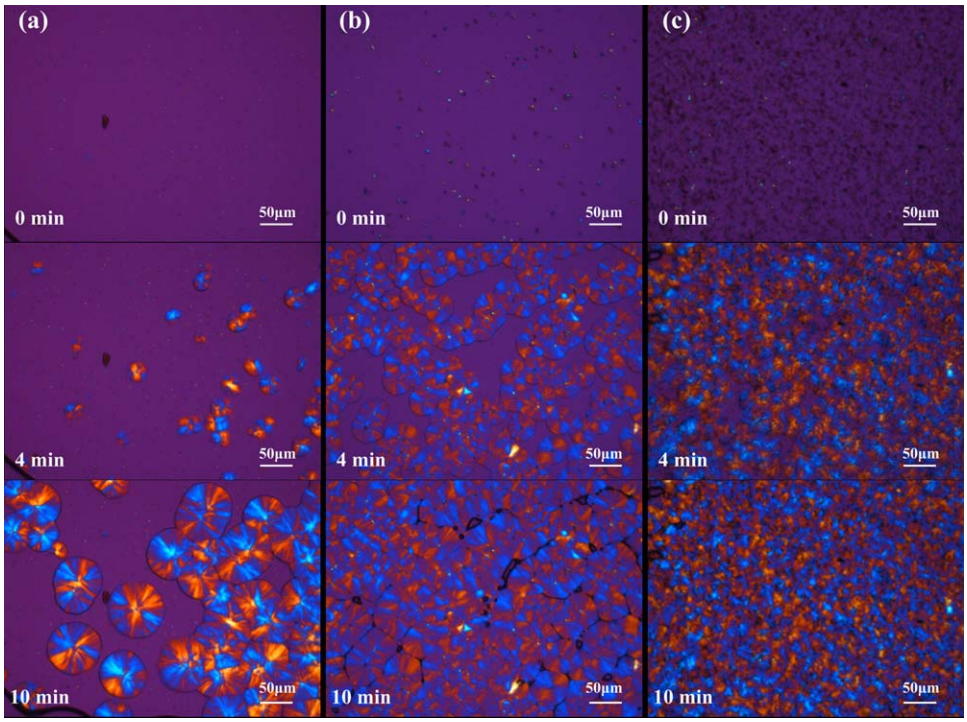

Figure 11. Polarized optical micrographs of (a) iPP; (b) iPP/DA-GO-5, and (c) iPP/DA-GO-50 during isothermally crystallizing at 132°C. [Color figure can be viewed in the online issue, which is available at wileyonlinelibrary.com.]

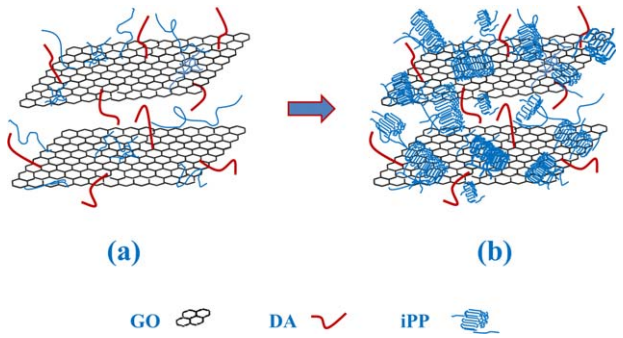

Figure 12. Schematic diagram of crystallization process of iPP/DA-GO nanocomposites. [Color figure can be viewed in the online issue, which is available at wileyonlinelibrary.com.]

sheet. Thus, some micro-scale nuclei can be observed in iPP/DA-GO nanocomposites at the beginning of the crystallization, as shown in Figure 12(a). Furthermore, it is reported that GO nanosheets have strong nucleation ability and can provide the area for crystallite nucleation.[45,46] In this study, DA-GO not only accelerates the crystallization process, but also enhances the crystalline ability. During the DA-GO induced crystallization process of iPP, iPP molecular chains can arrangement onto the GO nanosheets to form crystal [Figure 12(b)]. Therefore, the DA-GO in nanocomposites shows strong nucleation ability.

CONCLUSION

After hydrophobic GO was prepared by grafting dodecyl amine (DA), uniform dispersion of iPP/DA-GO nanocomposites were then prepared by solution mixing method. The isothermal crystallization behavior of iPP was efficiently accelerated by the addition of DA-GO and further promoted by the increase of DA-GO content, which was proved by the greatly reduced $t_{1/2}$, the significantly increased crystallization rate constant (K) and the considerably ascended equilibrium melting point (T_m^o). Moreover, the nucleation constant (K_g) of iPP/DA-GO-5 and iPP/DA-GO-50 were 5.7×10^5 and 11.6×10^5 K^2, respectively, much higher than that of neat iPP (5.3×10^5 K^2), which showed the strong nucleation ability of DA-GO. With respect to the non-isothermal crystallization behavior of iPP, the T_p of nanocomposites was obviously elevated. Additionally, the lower nucleation ability (Φ) and the decreased ΔEa value indicated that DA-GO as a nucleating agent can reduce the barrier to nucleation, which was caused by the surface interfacial free energy. The large nuclei density of iPP/DA-GO nanocomposites in POM micrographs further confirmed that the strong nucleation ability of DA-GO. This work may lay a foundation for further industrial applications of GO in polyolefin nanocomposites.

The authors thank the financial support by the National Foundation of China (Grant No. 51273161 and 21276168), the Opening Project of State Key Laboratory of Polymer Materials Engineering (Sichuan University) (KF201202).

REFERENCES

1. Li, R.; Liu, C. H.; Ma, J. *Carbohydr. Polym.* **2011**, *84*, 631.
2. Alvarez, V. A.; Pérez, C. J. *J. Therm. Anal. Calorim.* **2012**, *107*, 633.
3. Bora, C.; Dolui, S. K. *Polymer* **2012**, *53*, 923.
4. Huang, Y. W.; Zeng, M.; Ren, J.; Wang, J.; Fan, L. R.; Xu, Q. Y. *Colloids Surf. A: Physicochem. Eng. Aspects* **2012**, *401*, 97.
5. Kuila, T.; Bose, S.; Mishra, A. K.; Khanra, P.; Kim, N. H.; Lee, J. H. *Polym. Test.* **2012**, *31*, 31.
6. Lin, Y.; Jin, J.; Song, M. *J. Mater. Chem.* **2011**, *21*, 3455.
7. Jiang, X.; Drzal, L. T. *Compos. Part. A. Appl. Sci. Manuf.* **2011**, *42*, 1840.
8. Wang, G. X.; Shen, X. P.; Wang, B.; Yao, J.; Park, J. *Carbon* **2009**, *47*, 1359.
9. Zhang, L. B.; Wang, J. Q.; Wang, H. G.; Xu, Y.; Wang, Z. F.; Li, Z. P.; Mi, Y. J.; Yang, S. R. *Compos. Part. A. Appl. Sci. Manuf.* **2012**, *43*, 1537.
10. Yang, J. T.; Wu, M. J.; Chen, F.; Fei, Z. D.; Zhong, M. Q. *J. Supercrit. Fluids* **2011**, *56*, 201.
11. Veerapandian, M.; Lee, M. H.; Krishnamoorthy, K.; Yun, K. *Carbon* **2012**, *50*, 4228.
12. Paredes, J. I.; Villar-Rodil, S.; Martınez-Alonso, A.; Tascon, J. M. D. *Langmuir* **2008**, *24*, 10560.
13. Matsuo, Y.; Tahara, K.; Sugie, Y. *Cabron* **1997**, *35*, 113.
14. Satti, A.; Larpent, P.; Gun'ko, Y. *Carbon* **2010**, *48*, 3376.
15. Li, Y. Q.; Umer, R.; Samad, Y. A.; Zheng, L. X.; Liao, K. *Carbon* **2013**, *55*, 321.
16. Kim, Y. J.; Ha, S. T.; Lee, G. J.; Nam, J. H.; Ryu, I. H.; Nam, S. H.; Park, C. M.; In, I.; Kim, J.; Han, C. J. *J. Nanosci. Nanotechnol.* **2013**, *13*, 3464.
17. Kuila, T.; Bose, S.; Mishra, A. K.; Khanra, P.; Kim, N. H.; Lee, J. H. *Prog. Mater. Sci.* **2012**, *57*, 1061.
18. Gao, Y.; Chen, X. Q. Xu, H.; Zou, Y. L.; Gu, R. P.; Xu, M. S.; Jen, A. K. Y.; Chen, H. Z. *Carbon* **2010**, *48*, 4475.
19. Li, W. J.; Tang, X. Z.; Zhang, H. B.; Jiang, Z. G.; Yu, Z. Z.; Du, X. S.; Mai, Y. W. *Carbon* **2011**, *49*, 4724.
20. Song, P. A.; Liu, L.; Fu, S. Y.; Yu, Y. M.; Jin, C. D.; Wu, Q.; Zhang, Y.; Li, Q. *Nat. Nanotechnol.* **2013**, *24*, 1.
21. Moore, E. M.; Ortiz, D. L.; Marla, V. T.; Shambaugh, R. L.; Grady, B. P. *J. Appl. Polym. Sci.* **2004**, *93*, 2926.
22. Zhao, J. H. Dai, K.; Liu, C. G.; Zheng, G. Q.; Wang, B.; Liu, C. T.; Chen, J. B.; Shen, C. Y. *Compos. Part. A. Appl. Sci. Manuf.* **2013**, *48*, 129.
23. Pan, Y. Z.; Li, L.; Chan, S. H.; Zhao, J. H. *Compos. Part. A. Appl. Sci. Manuf.* **2010**, *41*, 419.
24. Qiu, S. C.; Zheng, Y. Y.; Zeng, A. R.; Guo, Y. *Thermochim. Acta.* **2011**, *512*, 28.
25. Papageorgiou, D. G.; Papageorgiou, G. Z.; Bikiaris, D. N.; Chrissafis, K. *Eur. Polym. J.* **2013**, *49*, 1577.
26. Assouline, E.; Lustiger, A.; Barber, A. H.; Cooper, C. A.; Klein, E.; Wachtel, E.; Wagner, H. D. *J. Polym. Sci. Part B. Polym. Phys.* **2003**, *41*, 520.
27. Valentini, L.; Biagiotti, J.; López-Manchado, M. A.; Santucci, S.; Kenny, J. M. *Polym. Eng. Sci.* **2004**, *44*, 303.
28. Xu, J. Z.; Liang, Y. Y.; Huang, H. D.; Zhong, G. J.; Lei, J.; Chen, C.; Li, Zh. M. *J. Polym. Res.* **2012**, *19*, 1.

29. Ferreira, C.I.; Castel, C. D.; Oviedo, M. A. S.; Mauler, R. S. *Thermochim. Acta.* **2013**, *553*, 40.
30. Ren, P. G.; Yan, D. X.; Ji, X.; Chen, T.; Li, Z. M. *Nanotechnology*, **2011**, *22*, 055705.
31. Ren, P. G.; Yan, D. X.; Chen, T.; Zeng, B. Q.; Li, Z. M. *J. Appl. Polym. Sci.*, **2011**, *121*, 3167.
32. Shi, X. M.; Wang, J. D.; Jiang, B. B.; Yang, Y. R. *J. Appl. Polym. Sci.* **2013**, *128*, 3609.
33. Avrami, M. *J. Chem. Phys.* **1939**, *7*, 1103.
34. Avrami, M. *J. Chem. Phys.* **1940**, *8*, 212.
35. Al-Hussein, M.; Strobl, G. *Macromolecules* **2002**, *35*, 1672.
36. Zou, P.; Tang, S. W.; Fu, Z. Z.; Xiong, H. G. *Int. J. Therm. Sci.* **2009**, *48*, 837.
37. Hoffman, J. D. Weeks, J. J. *J. Res. Natl Bur. Stand. A* **1962**, *66*, 13.
38. Ou, R. X.; Xie, Y. J.; Guo, C. G.; Wang, Q. W. *J. Appl. Polym. Sci.* **2012**, *126*, E2.
39. Huang, J. W.; Kang, C. C.; Chen, T. H. *J. Appl. Polym. Sci.* **2005**, *97*, 1051.
40. Hoffman, J. D.; Davis, G. T.; Lauritzen, J. I. Plenum, New York, **1976**.
41. Clark, E. J.; Hoffman, J. D. *Macromolecules* **1984**, *17*, 878.
42. Dobreva, A. Gutzow, I. *J. Non-Cryst. Solids.* **1993**, *162*, 1.
43. Kissinger H. E. *Anal. Chem.* **1957**, *29*, 1702.
44. Kang, J.; Li, J. P.; Chen, S. H.; Peng, H. M.; Wang, B.; Cao, Y.; Li, H. L.; Chen, J. Y.; Gai, J. G.; Yang, F.; Xiang, M. *J. Appl. Polym. Sci.* **2013**, *129*, 2663.
45. Xu, J. Z.; Chen, C.; Wang, Y.; Tang, H.; Li, Z. M.; Hsiao, B. S. *Macromolecules* **2011**, *44*, 2808.
46. Xu, J. Z.; Liang, Y. Y.; Zhong, G. J.; Li, H. L.; Chen, C.; Li, L. B.; Li, Z. M. *J. Phys. Chem. Lett.* **2012**, *3*, 530.